NeuroImage: Clinical 12 (2016) 707–714

Contents lists available at ScienceDirect

NeuroImage: Clinical

journal homepage: www.elsevier.com/locate/ynicl

A fractional motion diffusion model for grading pediatric brain tumors☆,☆☆

M. Muge Karaman, PhD[a], He Wang, PhD[e], Yi Sui, PhD[a,d], Herbert H. Engelhard, MD, PhD[c], Yuhua Li, MD[f,*,1], Xiaohong Joe Zhou, PhD[a,b,c,d,**,1]

[a]Center for MR Research, University of Illinois at Chicago, Chicago, IL, USA
[b]Department of Radiology, University of Illinois at Chicago, Chicago, IL, USA
[c]Department of Neurosurgery, University of Illinois at Chicago, Chicago, IL, USA
[d]Department of Bioengineering, University of Illinois at Chicago, Chicago, IL, USA
[e]Institute of Science and Technology for Brain-Inspired Intelligence, Fudan University, Shanghai, China
[f]Xinhua Hospital, Shanghai, China

ARTICLE INFO

Article history:
Received 29 July 2016
Received in revised form 30 September 2016
Accepted 1 October 2016
Available online 05 October 2016

Keywords:
Pediatric brain tumor
Non-Gaussian diffusion models
Anomalous diffusion
Fractional motion
Continuous-time random-walk
Tumor grading

ABSTRACT

Objectives: To demonstrate the feasibility of a novel fractional motion (FM) diffusion model for distinguishing low- versus high-grade pediatric brain tumors; and to investigate its possible advantage over apparent diffusion coefficient (ADC) and/or a previously reported continuous-time random-walk (CTRW) diffusion model.
Materials and methods: With approval from the institutional review board and written informed consents from the legal guardians of all participating patients, this study involved 70 children with histopathologically-proven brain tumors (30 low-grade and 40 high-grade). Multi-*b*-value diffusion images were acquired and analyzed using the FM, CTRW, and mono-exponential diffusion models. The FM parameters, D_{fm}, φ, ψ (non-Gaussian diffusion statistical measures), and the CTRW parameters, D_m, α, β (non-Gaussian temporal and spatial diffusion heterogeneity measures) were compared between the low- and high-grade tumor groups by using a Mann-Whitney-Wilcoxon *U* test. The performance of the FM model for differentiating between low- and high-grade tumors was evaluated and compared with that of the CTRW and the mono-exponential models using a receiver operating characteristic (ROC) analysis.
Results: The FM parameters were significantly lower ($p < 0.0001$) in the high-grade (D_{fm}: 0.81 ± 0.26, φ: 1.40 ± 0.10, ψ: 0.42 ± 0.11) than in the low-grade (D_{fm}: 1.52 ± 0.52, φ: 1.64 ± 0.13, ψ: 0.67 ± 0.13) tumor groups. The ROC analysis showed that the FM parameters offered better specificity (88% versus 73%), sensitivity (90% versus 82%), accuracy (88% versus 78%), and area under the curve (AUC, 93% versus 80%) in discriminating tumor malignancy compared to the conventional ADC. The performance of the FM model was similar to that of the CTRW model.
Conclusions: Similar to the CTRW model, the FM model can improve differentiation between low- and high-grade pediatric brain tumors over ADC.

1. Introduction

Among all pediatric cancers, brain tumors are the second most common, accounting for approximately 21–26% of cases (Ward et al., 2014; Kaatsch, 2010; American Cancer Society, 2016). Although the initial diagnosis of pediatric brain tumors is typically done by conventional magnetic resonance imaging (MRI), such as contrast-enhanced T_1-weighted imaging and unenhanced FLAIR, its role for accurately assessing tumor type, grade, and malignancy has not been fully established due to inadequate specificity (Kondziolka et al., 1993; Law et al., 2003). As such, invasive surgical biopsy followed by histopathological analysis continues to be the method of choice for tumor grading. For pediatric patients with brain tumor, however, surgical biopsy may not be always feasible because of the tumor locations (e.g., the brain stem), and biopsy always entails risks to the developing brain (Manoj et al., 2014; Albright et al.,

☆ Institutions where work originated: University of Illinois Hospital and Health Sciences System. Address: MC-707, Suite 1A, 1801 West Taylor Street, Chicago, Illinois 60612, USA; Xinhua Hospital Affiliated to Shanghai Jiaotong University School of Medicine. Address: 1665 Kongjiang Rd, Yangpu, Shanghai, China.
☆☆ This work was supported in part by grants from the National Institute of Health (1S10RR028898), the University of Illinois Center for Clinical and Translational Sciences, and Xinhua Hospital, Shanghai, China.
* Correspondence to: Yuhua. Li, Department of Radiology, Xinhua Hospital, Shanghai Jiaotong University School of Medicine, 1665 Kong Jiang Road, 200092 Shanghai, China.
** Correspondence to: Xiaohong Joe Zhou, Center for Magnetic Resonance Research and Departments of Radiology, Neurosurgery, and Bioengineering, University of Illinois at Chicago, 2242 West Harrison Street, Suite 103, M/C 831, Chicago, IL 60612, USA.
E-mail addresses: liyuhua10@sina.com (Y. Li), xjzhou@uic.edu (X.J. Zhou).
[1] Drs. Li and Zhou are the two senior authors who contributed equally to this work.

http://dx.doi.org/10.1016/j.nicl.2016.10.003

1993). Therefore, it would be highly desirable to have a noninvasive means of grading brain tumors.

Over the past decades, diffusion-weighted imaging (DWI) has been investigated for brain tumor grading based on the apparent diffusion coefficient (ADC) (Kono et al., 2001; Tien et al., 1994; Provenzale et al., 2006; Cha, 2006; Maier et al., 2010). This parameter, which is computed using a mono-exponential model (i.e., the Gaussian model), has been found to be sensitive to tissue cellularity changes associated with the neoplastic as well as other pathologic processes (Stadnik et al., 2001; Schaefer et al., 2000; Rowley et al., 1999; Moffat et al., 2005). This approach, however, has been increasingly challenged in recent years because water diffusion in tissues does not follow a Gaussian model, particularly at high b-values (e.g., $b \geq 1500$ s/mm^2). The mismatch between the mono-exponential model and the actual diffusion process is believed to be responsible, as least partially, for the substantial overlap in ADC values between low- and high-grade brain tumors (Kono et al., 2001; Maier et al., 2010; Yamasaki et al., 2005; Poretti et al., 2012).

Recognizing the limitations of conventional DWI with ADC, a number of researchers have developed more sophisticated diffusion models to better characterize "anomalous" (non-Gaussian) diffusion in biological tissues (Niendorf et al., 1996; Bennett et al., 2003; Yablonskiy et al., 2003; Assaf et al., 2000; Jensen et al., 2005; Magin et al., 2008; Zhou et al., 2010; Zhang et al., 2012; Assaf et al., 2004; Özarslan et al., 2006; Hall and Barrick, 2008; Alexander et al., 2002; De Santis et al., 2011; Karaman et al., 2015; Bai et al., 2016). Among these models, the continuous-time random-walk (CTRW) model and fractional motion (FM) model are of particular interest because they are regarded as the major "archrivals" by the biophysics community for describing the complex diffusion process in biological systems (Eliazar and Shlesinger, 2013). The CTRW model recognizes intra-voxel diffusion heterogeneity in both time and space, as characterized by diffusion waiting time and jump length, respectively (Karaman et al., 2015; Ingo et al., 2014). The FM model, on the other hand, describes the complex diffusion process based on the intricate statistical properties of water diffusion (Eliazar and Shlesinger, 2013; Fan and Gao, 2015). The properties obtained from these models can be related to the underlying microstructural and topological features of biological tissue either spatiotemporally, as in the CTRW model, or statistically, as in the FM model. These anomalous diffusion models provide new possibilities for improving tumor grading by probing the complexity, heterogeneity, and/or stochastic characteristics of the neoplastic tissues.

Several recent studies have shown that the CTRW model or its associated fractional order calculus (FROC) model offers substantial advantage over the mono-exponential diffusion model for differentiating low- versus high-grade brain tumors in both adult and pediatric patients (Karaman et al., 2015; Sui et al., 2015; Sui et al., 2016). Built upon this success, the present study aims at investigating whether the diffusion statistical properties revealed by the FM model can also be applied to differentiating low- from high-grade pediatric brain tumors, and whether the FM model offers an advantage over the mono-exponential and the CTRW models.

2. Materials and methods

2.1. Patient characteristics

Under the approval by the institutional review board of the performing hospital and with written informed consents from the legal guardians of all participating subjects, this prospective study enrolled a total of 73 children under the age of 18 years old. Inclusion criteria were: (a) presence of a newly diagnosed brain tumor without treatment; (b) availability of subsequent histopathological confirmation through biopsy; and (c) absence of neurologic disorders unrelated to the tumor. The exclusion criteria consisted of (a) contraindication to MRI examination; (b) excessive motion during the MRI scans; or (c) poor image quality due to hardware failure. Based on these criteria, three patients ($n = 3$) were excluded because of data corruption from excessive motion (>2 mm), resulting in a final patient group of 70 children, including 20 girls (4 months to 9 years old) and 50 boys (4 months to 13 years old). According to the World Health Organization (WHO) criteria (Louis et al., 2007), the 70 patients were divided into the low-grade (WHO grade I or II; $n = 30$; age range: 4 months to 13 years old; 7 girls) and high-grade (WHO grade III or IV; $n = 40$; age range: 4 months to 10 years old; 13 girls) tumor groups. Histopathologic analysis of the low-grade group revealed 10 pilocytic astrocytomas, 11 astrocytic astrocytomas, 3 ependymomas, 3 dysembryo plastic neuro epithelial tumors (DNET), and 3 choroid plexus papillomas. Histopathologies of the high-grade tumor group included 19 medulloblastomas, 4 teratoid/rhabdoid tumors (AT/RT), 2 glioblastoma multiformes (GBM), 4 germinomas, 2 pineoblastomas, 3 anaplastic ependymomas, 2 ependymoblastoma, 2 primitive neuroectodermal tumors (PNET), 1 anaplastic astrocytoma, and 1 malignant teratoma.

2.2. Image acquisition

MRI was performed on a 3-T scanner (Signa HDxt, GE Healthcare, Milwaukee, WI, USA) equipped with an 8-channel phased-array head coil (Invivo Corp., Gainesville, FL). All patients underwent conventional MRI, including pre- and post-contrast T1W imaging with FLAIR (TR/TE = 2200/22 ms, flip angle = 90°, TI = 860 ms, matrix size = 320 × 224, FOV = 22 cm × 22 cm, slice thickness = 5 mm), T2W imaging with fast spin echo (TR/TE = 3000/117 ms, echo train length = 24, matrix size = 320 × 224, FOV = 22 cm × 22 cm, slice thickness = 5 mm), and T2W FLAIR (TR/TE = 8000/120 ms, TI = 2250 ms, echo train length = 24, matrix size = 320 × 224, slice thickness = 5 mm, FOV = 22 cm × 22 cm). Before contrast administration, DWI with 12 b-values of 0, 10, 20, 50, 100, 200, 400, 800, 1200, 2000, 3000, and 4000 s/mm^2 was carried out using a single-shot spin-echo echo planar imaging (EPI) sequence (TR/TE = 4700/100 ms, acceleration factor = 2, separation between the Stejskal-Tanner gradient lobes (Δ) = 38.6 ms, duration of each diffusion gradient lobe (δ) = 32.2 ms, FOV = 22 cm × 22 cm, k-space matrix size = 128 × 128, image matrix size = 256 × 256, slice thickness = 5 mm, and the scan time ~3 min). In order to minimize the effect of diffusion anisotropy, trace-weighted images were obtained by successively applying the Stejskal-Tanner diffusion gradient along the x, y, and z directions at each non-zero b-value.

2.3. Diffusion models

The multi-b-value diffusion-weighted (DW) images were first analyzed by using the FM model in which the diffusion-attenuated MR signal was simplified as

$$S/S_0 = \exp\left(-\eta' D_{fm} b^{\frac{\varphi}{2}} \left(\Delta - \frac{\delta}{3}\right)^{-\frac{\varphi}{2}} \Delta^{\varphi+\psi} \delta^{-\varphi}\right), \quad (1)$$

based on the equations in (Fan and Gao, 2015). In Eq. (1), D_{fm} is an anomalous diffusion coefficient in mm^2/s, φ and ψ are the parameters governing the fluctuation and correlation properties of the increments of the diffusion process (Fan and Gao, 2015), δ and Δ are defined previously, and η' is a dimensionless factor to maintain nominal units (i.e., mm^2/s) for D_{fm}. The physical origins of the new statistical parameters, φ and ψ, are further explained in the Discussion section.

For comparison, the same DW images were also analyzed with the CTRW model whose diffusion-attenuated MR signal takes the following form:

$$S/S_0 = E_\alpha\left(-(bD_m)^\beta\right), \quad (2)$$

where D_m is an anomalous diffusion coefficient similar to D_{fm}, the parameters α and β are temporal and spatial fractional orders that are

related to temporal and spatial diffusion heterogeneities, respectively, and E_α is a Mittag-Leffler function (Karaman et al., 2015). For additional comparison, the conventional ADC values were also computed from a mono-exponential model given by

$$S/S_0 = \exp(-b\ ADC), \tag{3}$$

using b-values of 0 and 1200 mm^2/s, similar to what is done clinically.

2.4. Image analysis

The FM model parameters, D_{fm}, φ, and ψ, and the CTRW model parameters, D_m, α, and β, were estimated by fitting Eqs. (1) and (2) respectively to the same set of DW images on a voxel-by-voxel basis using a nonlinear least-squares estimation with an iterative Levenberg-Marquardt method in Matlab (MathWorks, Inc., Natick, MA). To filter out the pixels with low signal-to-noise ratio (SNR), a noise threshold was set at $n + 2\sigma$, where n and σ are the mean and standard deviation of the noise in the background, respectively (Zhou et al., 2010). Pixels with intensity below the threshold were not included in the calculation. The diffusion images, M_{raw}, were also corrected for Rician noise using $M_{rc} = \sqrt{M_{raw}^2 - 2\sigma_n^2}$, where M_{rc} is the Rician noise corrected signal and σ_n is standard deviation of the real or imaginary components of the noise. The noise bias, $2\sigma_n^2$, can be calculated as the average value of the magnitude squared signal of the background (Miller and Joseph, 1993). After filtering out the noise and correcting for Rician noise distribution, the anomalous diffusion coefficients, D_{fm} or D_m, were estimated by an exponential model using the diffusion images at b-values up to 3000 s/mm^2. With the estimated value of D_{fm} or D_m at each voxel, φ and ψ for the FM model, or α and β, for the CTRW model, were simultaneously estimated through a non-linear fitting, using all data with b-values from 0 to 4000 s/mm^2. This approach equalizes D_{fm} and D_m, allowing us to focus on comparison of the remaining anomalous diffusion parameters between the two models. The computation times of the FM (~1 min) and CTRW models (~2 min) were similar for one slice.

Guided by the high-resolution T1W, T2W, and FLAIR images, regions of interest (ROIs) were placed on the solid region of tumors in the images with $b = 0$, by excluding hemorrhage, cystic change, and/or necrosis on the T2W EPI images (i.e., images with $b = 0$). Solid-appearing non-enhancing tumor was also included in ROI selections. The selected ROIs were propagated to the corresponding D_{fm} (D_m), φ, ψ, α, β, and ADC maps for statistical analyses.

2.5. Statistical analyses

The mean D_{fm} (or D_m), φ, ψ, α, β, and ADC values in the tumor ROIs across all tumor-containing slices for each patient were obtained. For each patient group, the individual mean values were combined over all patients in the group to compute the descriptive statistics. The low- and high-grade tumor groups were then compared by a non-parametric Mann-Whitney-Wilcoxon U test.

The group comparison was performed using a receiver operating characteristic (ROC) analysis to evaluate the FM, CTRW, and mono-exponential models for differentiating low- and high-grade tumors. In addition to evaluating the performance of each individual parameter, different combinations of the FM parameters, (D_{fm}, φ), (D_{fm}, ψ), (φ, ψ), (D_{fm}, φ, ψ), and CTRW parameters, (D_m, α), (D_m, β), (α, β), (D_m, α, β), were evaluated using a multivariate logistic regression analysis (Gortmaker et al., 1994). This method estimates the probability of being a high-grade tumor, P_0, by using the following logistic functions for the FM model,

$$P_0 = \exp(a_0 + a_1 D_{fm} + a_2\varphi + a_3\psi)/[1 + \exp(a_0 + a_1 D_{fm} + a_2\varphi + a_3\psi)], \tag{4}$$

where a_0 is a constant and a_i (for $i = 1,2,3$) are the regression coefficients of the corresponding FM parameters. The probability P_0 for the CTRW model can be expressed analogously. These probability values were used as the test variables in the ROC analysis where the state variable was considered to be the 'true' tumor category obtained from histopathology. The best cut-off sensitivity and specificity values of the ROC curves were determined by using Youden's index that maximizes the sum of sensitivity and specificity. The performance of the models for tumor grade differentiation was subsequently compared by these sensitivity and specificity cut-off values as well as the diagnostic accuracy and the area under the curve (AUC).

3. Results

3.1. Comparison of representative patients from each group

Fig. 1 shows a set of representative parameter maps (FM parameters, φ and ψ, CTRW parameters, α and β, and diffusion coefficients, D_{fm} or D_m and ADC) obtained from a low-grade patient (3 year-old girl, WHO grade I, pilocytic astrocytoma; top two rows) and a high-grade patient (7 year-old boy, WHO grade IV, medulloblastoma; bottom two rows). All FM model parameters of the high-grade tumors (Fig. 1*c*, *d*, and *k*) were substantially lower than those of the low-grade tumors (Fig. 1*a*, *b*, and *i*) whereas the parametric values in the background brain parenchyma were essentially identical between the low- and the high-grade brain tumor patients. This result was consistent with the comparison of the ADC map between the low-grade (Fig. 1*j*) and the high-grade patient (Fig. 1*l*). Similar contrasts were observed in the parameter maps of the CTRW model in which the voxel values in the high-grade parameter maps (Fig. 1*g*, *h*, and *k*) are lower than those in the low-grade ones (Fig. 1*e*, *f*, and *i*).

3.2. Group comparison for tumor differentiation

Table 1 summarizes the descriptive statistics, including means and standard deviations, of the FM, CTRW, and mono-exponential model parameters computed over the tumor ROIs from all patients in each tumor group. All model parameters were found to be significantly lower in the high-grade than in the low-grade tumor group (p-values < 0.0001). The group separation is further demonstrated by the box and whisker plots of the mean FM (Fig. 2*a*, *d*, *e*) and CTRW (Fig. 2*a*, *b*, *c*) model parameters as well as the ADC value (Fig. 2*f*). Compared to the FM and CTRW model parameters, ADC value yielded more overlap between the two tumor groups (Fig. 2*f*). The statistically significant difference in the FM parameters (Fig. 2*a*, *d*, *e*) between the low- and high-grade tumor groups as well as the individual subject-level comparison in Fig. 1*a*–*d*, *i*, and *k* indicates that the FM model is useful for tumor differentiation. The comparisons in Table 1 as well as Figs. 1 and 2 suggest that the FM model and the CTRW model produced comparable results.

The ROC curves, which illustrate the performance of the individual and combination of FM or CTRW model parameters for differentiating low-grade (negative) and high-grade (positive) pediatric brain tumors, are given in Figs. 3 and 4, respectively. The best cut-off sensitivity and specificity values of the ROC curves are indicated by the filled circles. For comparison, the ROC curve for ADC is included in both figures. The performance metrics are summarized in Table 2 for the individual parameters, and in Tables 3 and 4 for the combined model parameters.

In the individual parameter analysis shown in Fig. 3 and Table 2, it was observed that both models outperformed the ADC value. Importantly, the relatively low specificity of ADC (0.733), which was also reported in other studies (Kono et al., 2001; Maier et al., 2010; Yamasaki et al., 2005; Poretti et al., 2012), was improved by several new model parameters (0.766 for ψ; 0.800 for α or β).

The performance for differentiating low- versus high-grade tumors was further improved by the use of combinations of the FM or CTRW model parameters. For the FM model shown in Fig. 4*a* and Table 3, the

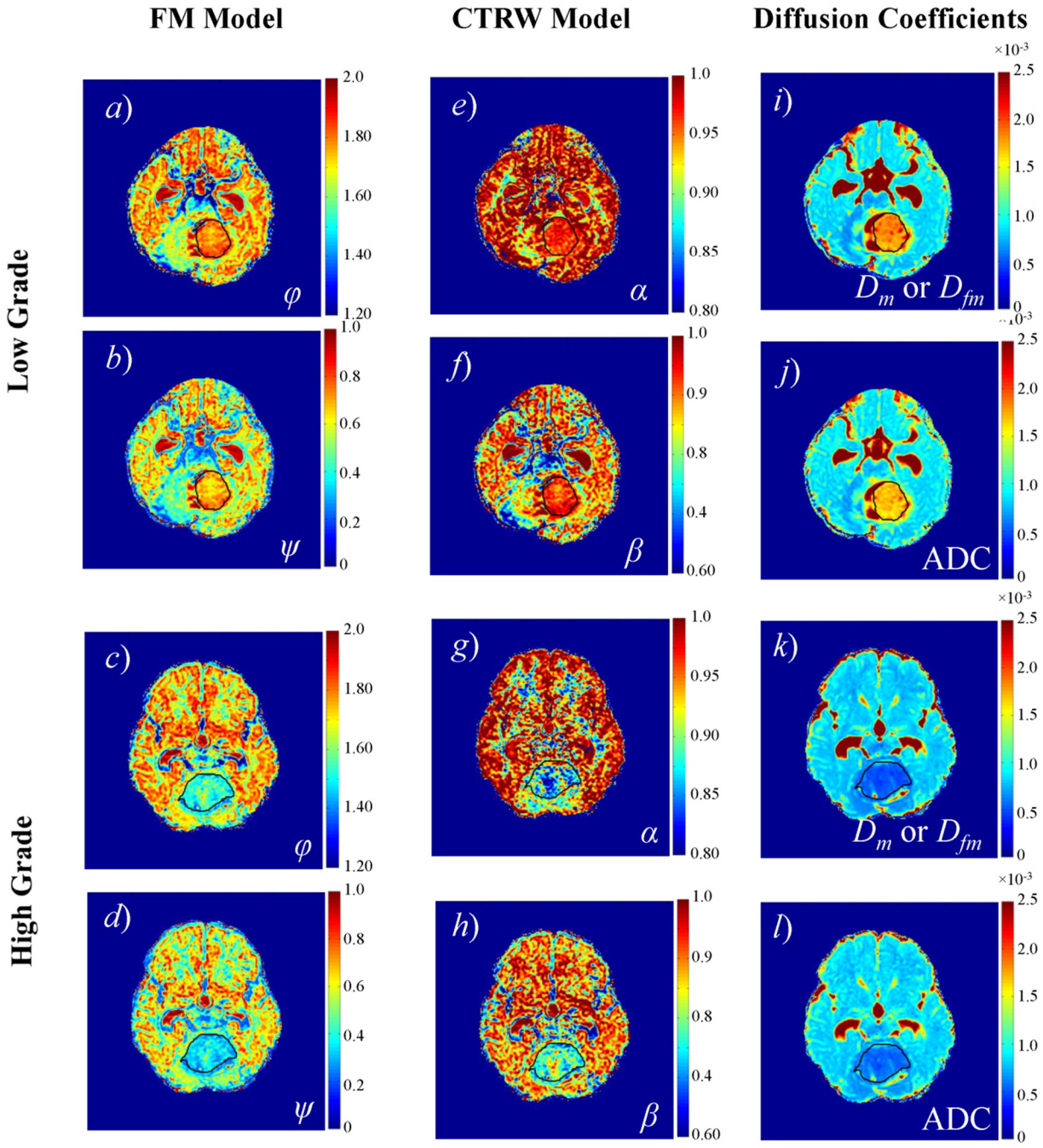

Fig. 1. Parameter maps from one representative low-grade patient (3 years old, WHO grade I, pilocytic astrocytoma) in the top two rows and one representative high-grade patient (7 years old, WHO grade IV, medulloblastoma) in the bottom two rows. *First column*: the FM parameters φ (*a* and *c*) and ψ (*b* and *d*); *second column:* the CTRW parameters α (*e* and *g*) and β (*f* and *h*); *third column:* anomalous diffusion parameters of the FM and CTRW models, D_m or D_{fm} (*i* and *k*) and ADC (*j* and *l*). The solid tumor ROIs, initially drawn on the T2W EPI image with the aid of T1W images, are shown with black contours in all images. All the parameter values within the ROIs are higher in the low-grade patient compared to those from the high-grade patient given.

Table 1
Descriptive statistics, showing sample mean and standard deviation, ($\bar{x} \pm \sigma$), of the FM and CTRW model parameters and the ADC values for the low-grade (LG) and high-grade (HG) tumor groups.

	D_{fm} or D_m (in μm^2/ms)	φ	ψ	α	β	ADC (in μm^2/ms)
LG ($n = 30$)	1.52 ± 0.52	1.64 ± 0.13	0.67 ± 0.13	0.94 ± 0.03	0.91 ± 0.06	0.92 ± 0.32
HG ($n = 40$)	0.81 ± 0.26	1.40 ± 0.10	0.42 ± 0.11	0.90 ± 0.03	0.81 ± 0.05	0.60 ± 0.18
p-Value	$p < 0.0001$	$p < 0.0001$	$p < 0.0001$	$p < 0.0001$	$p < 0.0001$	$p < 0.0001$

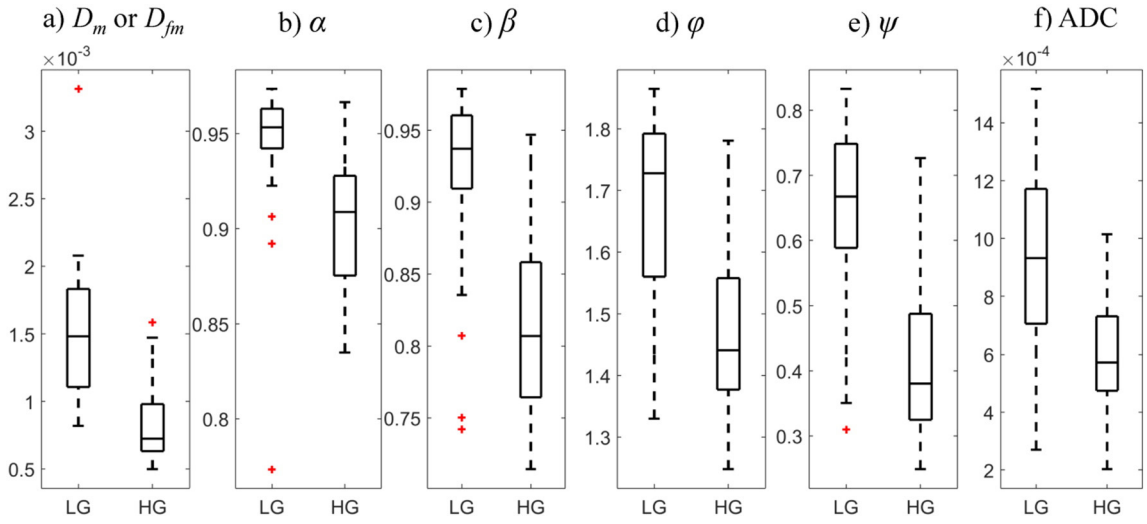

Fig. 2. Box and whisker plots of mean values of the FM and CTRW parameters, D_{fm} or D_m in *a*), α in *b*), β in *c*), φ in *d*), ψ in *e*), and of the ADC value in *f*) for low- and high-grade pediatric brain tumors. The central boxes represent the values from the lower to upper quartile whereas the middle line represents the median. The red "+" symbol denotes the outliers that are >1.5 times the interquartile range from the quartiles. Both the FM and CTRW parameters exhibited a statistically significant difference between the low- and high-grade pediatric brain tumor groups with *p*-values < 0.0001.

combination of (D_{fm}, φ, ψ) yielded the best specificity (0.885), sensitivity (0.900), accuracy (0.885), and AUC (0.934). For the CTRW model, both (D_m, α, β) and (D_m, α) yielded the best specificity (0.866), sensitivity (0.850), accuracy (0.857), and AUC (0.924) compared to the other combinations of the CTRW parameters as shown in Fig. 4*b* and Table 4. Overall, the FM and the CTRW models produced comparable performance that was superior to the mono-exponential model with ADC, particularly in specificity (0.733 versus 0.885 and 0.866), accuracy (0.785 versus 0.885 and 0.857), and AUC (0.801 versus 0.934 and 0.923) as given in the last column of Table 2.

4. Discussion

In this study, we have demonstrated that a novel diffusion model, the FM model, can provide a set of parameters (D_{fm}, φ, ψ) that improved MR-based differentiation between low- and high-grade pediatric brain tumors as compared to conventional ADC. Furthermore, comparison between the FM model with another recently introduced diffusion model, the CTRW model, showed that the performance of the two models is similar for distinguishing low- versus high grade pediatric brain tumors. The improvements achieved by the FM and CTRW models over the mono-exponential model may be important for pediatric brain tumors where surgical biopsy can be difficult to perform due to the tumor locations (e.g., the brain stem) with elevated risks to the developing brain.

The need for non-invasive, image-based tumor grading and the sub-optimal performance of conventional MRI have led to an increasing number of DWI studies on brain tumor characterization. While the ADC values from the popular mono-exponential diffusion model have been found useful (Stadnik et al., 2001; Schaefer et al., 2000; Rowley et al., 1999), a number of studies have also reported significant overlap

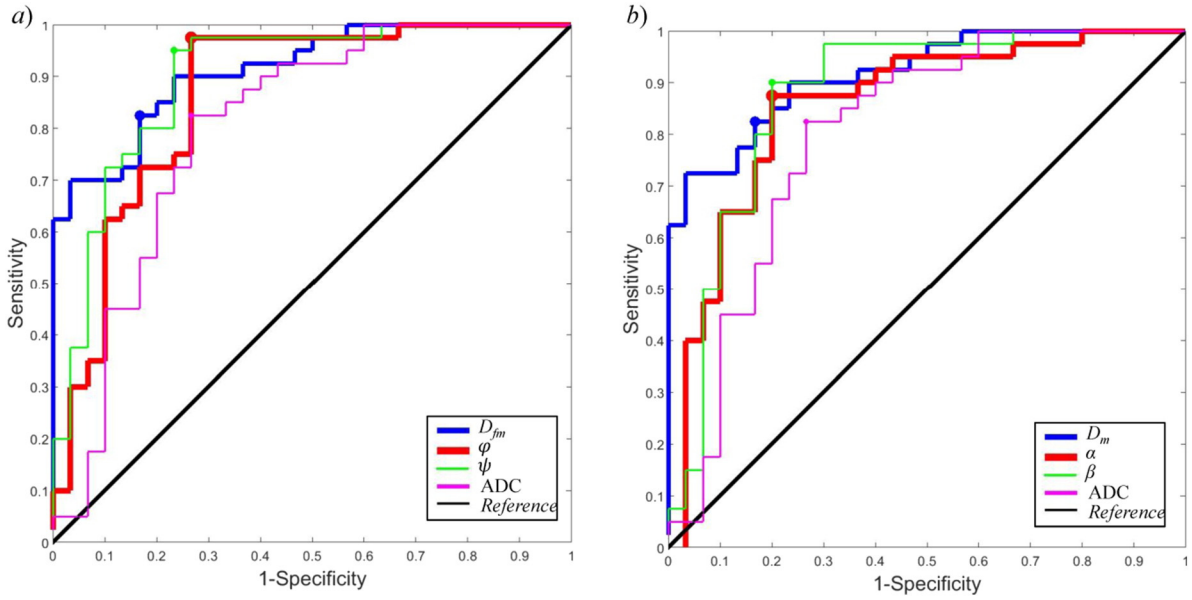

Fig. 3. The ROC curves of using individual FM parameters, D_{fm}, φ, and ψ, in *a*), and the CTRW parameters, D_m, α, and β, in *b*) for differentiating between low- and high-grade pediatric brain tumors. The best cut-off sensitivity and specificity values for each ROC curve are indicated by the filled circles. The AUCs for the corresponding ROC curves are 0.913 (D_{fm}), 0.864 (φ), and 0.897 (ψ) for the FM model and 0.913 (D_m), 0.855 (α), and 0.875 (β) for the CTRW model. For comparison, the ROC curve of ADC is included in both *a*) and *b*).

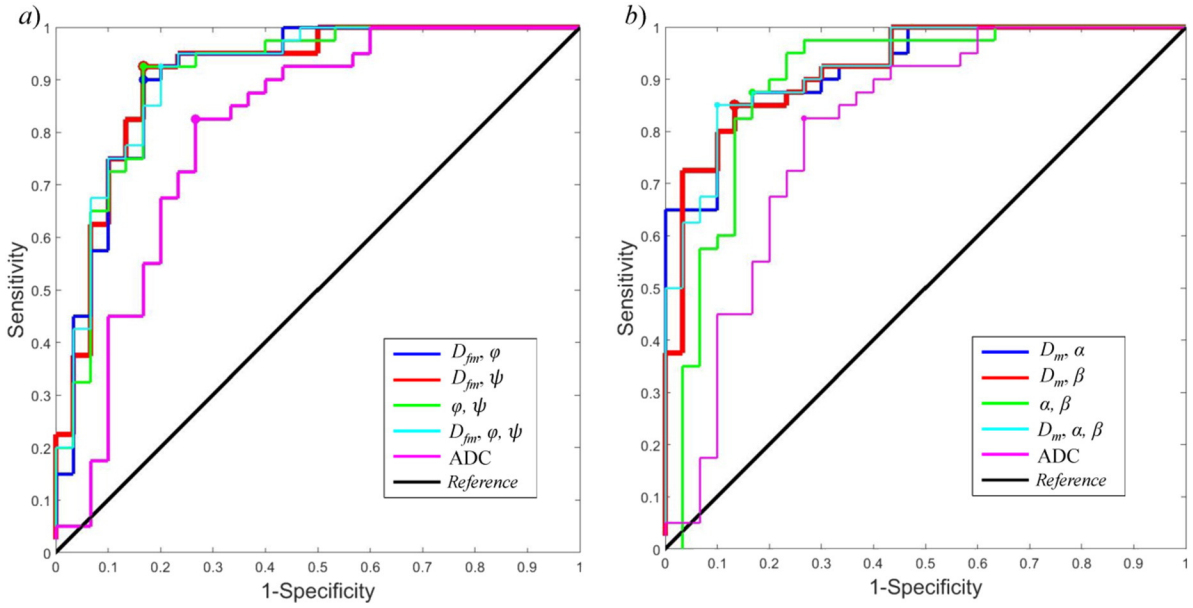

Fig. 4. The ROC curves of using the different combinations of the FM parameters (D_{fm}, φ, ψ) in *a*), and the CTRW parameters (D_m, α, β) in *b*) for differentiating between low- and high-grade pediatric brain tumors. The best cut-off sensitivity and specificity values for each ROC curve are indicated by the filled circles. The AUCs for the corresponding ROC curves are 0.927 (D_{fm} and φ), 0.933 (D_{fm} and ψ), 0.921 (φ and ψ), 0.934 (D_{fm}, φ, and ψ) for the FM model, 0.924 (D_m and α), 0.921 (D_m and β), 0.895 (α and β), 0.923 (D_m, α, and β) for the CTRW model, and 0.801 (ADC). For comparison, the ROC curve of ADC is included in both *a*) and *b*).

in ADC values between different tumor grades, reducing the overall specificity and accuracy (Kono et al., 2001; Maier et al., 2010; Yamasaki et al., 2005; Poretti et al., 2012; Bai et al., 2016).

To overcome the limitation, a number of non-Gaussian diffusion models have been developed over the last decades (Niendorf et al., 1996; Bennett et al., 2003; Yablonskiy et al., 2003; Assaf et al., 2000; Jensen et al., 2005; Magin et al., 2008; Zhou et al., 2010; Zhang et al., 2012; Assaf et al., 2004; Özarslan et al., 2006; Hall and Barrick, 2008; Alexander et al., 2002; De Santis et al., 2011; Karaman et al., 2015; Bai et al., 2016; Ingo et al., 2014; Sui et al., 2015; Sui et al., 2016; Winfeld et al., 2013; Jiang et al., 2015). For example, diffusion kurtosis imaging (DKI) has been applied to brain tumor grading for both pediatric (Winfeld et al., 2013) and adult patients (Jiang et al., 2015). A recent study by Bai et al. (Bai et al., 2016) demonstrated excellent performance of an empirical heterogeneity index from the stretched-exponential model for glioma grading in adults. The underlying premise is that high-grade gliomas have an elevated level of tissue heterogeneity. This result reinforces an earlier study on characterizing high-grade gliomas using the empirical heterogeneity index (Kwee et al., 2010). However, both studies relied on the *empirical* stretched-exponential model. The empirical nature is eliminated by the CTRW model where structural heterogeneity is directly related to two different aspects of the anomalous diffusion process: diffusion heterogeneity in time (represented by α) and space (represented by β) (Magin et al., 2008; Zhou et al., 2010; Karaman et al., 2015; Gao et al., 2011). Several recent studies have indicated that the CTRW model and its associated FROC model can improve the specificity and diagnostic accuracy over ADC in differentiating brain tumor grades because of their ability to probe diffusion heterogeneities (Karaman et al., 2015; Sui et al., 2015; Sui et al., 2016).

In parallel to the CTRW and FROC models, the FM model has attracted an increasing attention in the biophysics community over recent years (Eliazar and Shlesinger, 2013; Weiss, 2013; Szymanski and Weiss, 2009; Magdziarz et al., 2009; Ernst et al., 2012). Several studies (Weiss, 2013; Szymanski and Weiss, 2009; Magdziarz et al., 2009; Ernst et al., 2012) have concluded that fractional motion is more likely the underlying process in biological systems; and water diffusion does *not* follow the dynamics of CTRW. These studies, however, were conducted either in cell culture or on individual molecules. The validity of their conclusions remains unexplored for DWI where diffusion behavior at a scale of an image voxel (e.g., $2 \times 2 \times 3$ mm^3) must be considered. The present study is among the first of such effort. Our study has shown that the FM and CTRW models performed equally well in differentiating between low- and high-grade pediatric brain tumors. This seemingly surprising result can be attributed to the fact that voxel-level averaging, instead of individual molecular or cellular behavior, dominates water diffusion behavior in DWI. At the voxel level, tissue heterogeneity and structural complexity provide a completely different diffusion environment than that for individual molecules in cell cultures. This environmental difference is further pronounced in brain tumors where extensive tissue heterogeneity (necrosis, cyst, hemorrhage, edema, and/or calcification) and structural complexity (capillaries, different cell types, and/or cellularity) exist. The tissue heterogeneity in a DWI voxel is primarily related to these tissue features which have typical dimensions much larger than the maximum diffusion path length probed by the diffusion time in a DWI pulse sequence. The measured average diffusion parameters in the tissue culture, on the

Table 2
Sensitivity, specificity, diagnostic accuracy, and the AUC of the ROC analysis for the individual FM and CTRW model parameters and the ADC value for tumor differentiation.

	D_{fm} or D_m	φ	ψ	α	β	ADC
Specificity cut-off	0.833	0.733	0.766	0.800	0.800	0.733
Sensitivity cut-off	0.825	0.975	0.950	0.875	0.900	0.825
Accuracy	0.828	0.871	0.871	0.842	0.857	0.785
AUC	0.913	0.864	0.897	0.855	0.875	0.801

Table 3
Sensitivity, specificity, diagnostic accuracy, and the AUC of the ROC analysis for the different combinations of the FM parameters for tumor differentiation.

	(D_{fm}, φ)	(D_{fm}, ψ)	(φ, ψ)	(D_{fm}, φ, ψ)
Specificity cut-off	0.866	0.866	0.800	0.885
Sensitivity cut-off	0.875	0.875	0.950	0.900
Accuracy	0.871	0.871	0.885	0.885
AUC	0.927	0.933	0.921	0.934

Table 4
Sensitivity, specificity, diagnostic accuracy, and the AUC of the ROC analysis for the different combinations of the CTRW parameters for tumor differentiation.

	(D_m, α)	(D_m, β)	(α, β)	(D_m, α, β)
Specificity cut-off	0.866	0.866	0.833	0.866
Sensitivity cut-off	0.850	0.850	0.875	0.850
Accuracy	0.857	0.857	0.857	0.857
AUC	0.924	0.921	0.895	0.923

other hand, reflect the diffusion environment at a much smaller spatial scale. Therefore, it is not surprising that the drastic difference between the FM and CTRW models reported by the biophysical community were not observed in this DWI study.

Our simplification of the FM model has yielded two new parameters, φ and ψ. The φ parameter governs the fluctuations of the diffusion process by determining the variance properties of the increments which can be finite (mild fluctuations) or infinite (wild fluctuations). Thus, φ characterizes the diffusion as either a Gaussian or a Levy process according to the FM theory (Eliazar and Shlesinger, 2013). The ψ parameter, on the other hand, describes the correlation properties of the diffusion increments as positively correlated (long-range), negatively correlated (short-range), or not correlated (no memory). As such, ψ determines whether the underlying anomalous diffusion process is a Gaussian/Levy or fractional Gaussian/Levy process (Eliazar and Shlesinger, 2013). As both aspects originate from intra-voxel diffusion heterogeneity, it is plausible that the FM and CTRW models would produce similar results. Their similar performance observed in this study suggests that both the FM parameters (D_{fm}, φ, ψ) and the CTRW parameters (D_m, α, β) can be sensitive to changes in tissue structures as the degree of malignancy progresses. High-grade tumors exhibited lower φ and ψ values, indicating an increased degree of structural complexity (e.g., increased capillaries, presence of edema, necrosis, hemorrhage, etc.) that led to elevated non-Gaussian diffusion characteristics. This increased tissue complexity was also captured by the CTRW model parameters (α, β), as shown in this study as well as an earlier study (Karaman et al., 2015). The FM parameters may reflect either similar diffusion heterogeneity to the CTRW parameters or other complementary aspects of tissue structural complexity. The exact relationship between the FM parameters and tissue structure complexity remains to be established and may be better understood through extensive computer simulations and histopathologic correlations.

The comparable results of the FM and CTRW models for differentiating neoplastic pathology are one of the key outcomes of this study. The similarity of their performances in tumor ROI, despite the differences in the theoretical bases and mathematical representations, suggests that both models can equally capture the structural complexity from a high *b*-value data set acquired under the current acceptable clinical settings. These models can be further evaluated in the living human tissue under more advanced imaging conditions, such as higher *b*-values beyond 4000 s/mm^2 and varying diffusion times, to provide new insights into the tissue structures. Such similarity also implies that simplification or consolidation of the non-Gaussian diffusion modeling may be possible without losing the advantages in sensitivity, specificity, and accuracy.

Our study has several limitations. First, no numerical simulations, phantom experiments, or histologic correlations with known structures were attempted to validate the FM model parameters. Second, our study does not include a normal control group. Instead, the normal appearing gray matter on the contralateral side of the tumor was employed as an internal control, and no significant difference was found between the two tumor groups ($p > 0.10$). Third, the maximal *b*-value used in the FM or CTRW analysis was different from that employed in the ADC analysis. Hence, the SNR at the highest *b*-value can differ by about 2.6 times. Even with this SNR disadvantage, the CTRW and FM models outperformed the mono-exponential model. This performance is expected to improve further if the SNRs of the DW images are matched. Lastly, we divided the patients only into two groups, low-grade and high-grade, without further classifying them into the individual grades or sub-types. This was primarily due to the moderate number of patients enrolled in the study.

In conclusion, we have demonstrated the feasibility of using an FM diffusion model with high *b*-values to improve differentiating between low- and high-grade pediatric brain tumors over the conventional ADC approach, offering higher specificity (88%), sensitivity (90%), and diagnostic accuracy (88%). Moreover, we have shown that the FM and CTRW models provide similar performance for discriminating the malignancy of pediatric brain tumors, which challenges several recent reports on the drastic difference between the two models observed in cell cultures. Although the biophysical origin of the FM model requires further investigation, this model can provide a new avenue for grading brain tumors noninvasively in pediatric patients.

Acknowledgements

This work was supported in part by a grant from the National Institutes of Health (Grant No. 1S10RR028898). The authors are grateful to Drs. Richard L. Magin, Kejia Cai, Keith R. Thulborn, and Ying Xiong for helpful discussions. YL and XJZ contributed equally to this work and share the senior authorship.

References

Albright, A.L., Packer, R.J., Zimmerman, R., Rorke, L.B., Boyett, J., Hammond, G.D., et al., 1993. Magnetic resonance scans should replace biopsies for the diagnosis of diffuse brain stem gliomas: a report from the Children's Cancer Group. Neurosurgery 33 (6), 1026–1030.
Alexander, D.C., Barker, G.J., Arridge, S.R., 2002. Detection and modeling of non-Gaussian apparent diffusion coefficient profiles in human brain data. Magn. Reson. Med. 48 (2), 331–340.
American Cancer Society, 2016. Cancer Facts & Figures 2016. Atlanta, GA.
Assaf, Y., Mayk, A., Cohen, Y., 2000. Displacement imaging of spinal cord using q-space diffusion-weighted MRI. Magn. Reson. Med. 44, 713–722.
Assaf, Y., Freidlin, R.Z., Rohde, G.K., Basser, P.J., 2004. New modeling and experimental framework to characterize hindered and restricted water diffusion in brain white matter. Magn. Reson. Med. 52 (5), 965–978.
Bai, Y., Lin, Y., Tian, J., Shi, D., Cheng, J., Haacke, E.M., et al., 2016. Grading of gliomas by using monoexponential, biexponential, and stretched exponential diffusion-weighted MR imaging and diffusion kurtosis MR imaging. Radiology 278 (2), 496–504.
Bennett, K.M., Schmainda, K.M., Bennett, R., Rowe, D.B., Lu, H., Hyde, J.S., 2003. Characterization of continuously distributed cortical water diffusion rates with a stretched-exponential model. Magn. Reson. Med. 50, 727–734.
Cha, S., 2006. Update on brain tumor imaging: from anatomy to physiology. Am. J. Neuroradiol. 27, 475–487.
De Santis, S., Gabrielli, A., Palombo, M., Maraviglia, B., Capuani, S., 2011. Non-Gaussian diffusion imaging: a brief practical review. Magn. Reson. Imaging 29 (10), 1410–1416.
Eliazar, I.I., Shlesinger, M.F., 2013. Fractional motions. Phys. Rep. 527 (2), 101–129.
Ernst, D., Hellmann, M., Köhler, J., Weiss, M., 2012. Fractional Brownian motion in crowded fluids. Soft Matter 8 (18), 4886–4889.
Fan, Y., Gao, J.-H., 2015. Fractional motion model for characterization of anomalous diffusion from NMR signals. Phys. Rev. E 92 (1), 012707.
Gao, Q., Srinivasan, G., Magin, R.L., Zhou, X.J., 2011. Anomalous diffusion measured by a twice-refocused spin echo pulse sequence: analysis using fractional order calculus. J. Magn. Reson. Imaging 33 (5), 1177–1183.
Gortmaker, S.L., Hosmer, D.W., Lemeshow, S., 1994. Applied logistic regression. Contemp Sociol. 159.
Hall, M.G., Barrick, T.R., 2008. From diffusion-weighted MRI to anomalous diffusion imaging. Magn. Reson. Med. 59 (3), 447–455.
Ingo, C., Magin, R.L., Colon-Perez, L., Triplett, W., Mareci, T.H., 2014. On random walks and entropy in diffusion-weighted magnetic resonance imaging studies of neural tissue. Magn. Reson. Med. 71 (2), 617–627.
Jensen, J.H., Helpern, J.A., Ramani, A., Lu, H., Kaczynski, K., 2005. Diffusional kurtosis imaging: the quantification of non-Gaussian water diffusion by means of magnetic resonance imaging. Magn. Reson. Med. 53, 1432–1440.
Jiang, R., Jiang, J., Zhao, L., Zhang, J., Zhang, S., Yao, Y., et al., 2015. Diffusion kurtosis imaging can efficiently assess the glioma grade and cellular proliferation. Oncotarget 6 (39), 42380–42393.
Kaatsch, P., 2010. Epidemiology of childhood cancer. Cancer Treat. Rev. 36 (4), 277–285.
Karaman, M.M., Sui, Y., Wang, H., Magin, R.L., Li, Y., Zhou, X.J., 2015. Differentiating low- and high-grade pediatric brain tumors using a continuous-time random-walk diffusion model at high b-values. Magn Reson Med [Internet] (Available from: 10.1002/mrm.26012).
Kondziolka, D., Lunsford, L.D., Martinez, A.J., 1993. Unreliability of contemporary neurodiagnostic imaging in evaluating suspected adult supratentorial (low-grade) astrocytoma. J. Neurosurg. 79 (4), 533–536.

Kono, K., Inoue, Y., Nakayama, K., Shakudo, M., Morino, M., Ohata, K., et al., 2001. The role of diffusion-weighted imaging in patients with brain tumors. Am. J. Neuroradiol. 22 (6), 1081–1088.
Kwee, T.C., Galbán, C.J., Tsien, C., Junck, L., Sundgren, P.C., Ivancevic, M.K., et al., 2010. Intravoxel water diffusion heterogeneity imaging of human high-grade gliomas. NMR Biomed. 23 (2), 179–187.
Law, M., Yang, S., Wang, H., Babb, J.S., Johnson, G., Cha, S., et al., 2003. Glioma grading: sensitivity, specificity, and predictive values of perfusion MR imaging and proton MR spectroscopic imaging compared with conventional MR imaging. Am. J. Neuroradiol. 24, 1989–1998.
Louis, D.N., Ohgaki, H., Wiestler, O.D., Cavenee, W.K., Burger, P.C., Jouvet, A., et al., 2007. The 2007 WHO classification of tumours of the central nervous system. Acta Neuropathol. 114 (2), 97–109.
Magdziarz, M., Weron, A., Burnecki, K., Klafter, J., 2009. Fractional Brownian motion versus the continuous-time random walk: a simple test for subdiffusive dynamics. Phys. Rev. Lett. 103 (18), 1–4.
Magin, R.L., Abdullah, O., Baleanu, D., Zhou, X.J., 2008. Anomalous diffusion expressed through fractional order differential operators in the Bloch-Torrey equation. J. Magn. Reson. Imaging 190, 255–270.
Maier, S.E., Sun, Y., Mulkern, R.V., 2010. Diffusion imaging of brain tumors. NMR Biomed. 23 (7), 849–864.
Manoj, N., Arivazhagan, A., Bhat, D.I., Arvinda, H.R., Mahadevan, A., Santosh, V., et al., 2014. Stereotactic biopsy of brainstem lesions: techniques, efficacy, safety, and disease variation between adults and children: a single institutional series and review. J. Neurosci. Rural Prac. 5 (1), 32–39.
Miller, A.J., Joseph, P.M., 1993. The use of power images to perform quantitative analysis on low SNR MR images. Magn. Reson. Imaging 11 (7), 1051–1056.
Moffat, B.A., Chenevert, T.L., Lawrence, T.S., Meyer, C.R., Johnson, T.D., Dong, Q., et al., 2005. Functional diffusion map: a noninvasive MRI biomarker for early stratification of clinical brain tumor response. Proc. Natl. Acad. Sci. U. S. A. 102, 5524–5529.
Niendorf, T., Dijkhuizen, R.M., Norris, D.G., van Lookeren, C.M., Nicolay, K., 1996. Biexponential diffusion attenuation in various states of brain tissue: implications for diffusion-weighted imaging. Magn. Reson. Med. 36, 847–857.
Özarslan, E., Basser, P.J., Shepherd, T.M., Thelwall, P.E., Vemuri, B.C., Blackband, S.J., 2006. Observation of anomalous diffusion in excised tissue by characterizing the diffusion-time dependence of the MR signal. J. Magn. Reson. 183 (2), 315–323.
Poretti, A., Meoded, A., Huisman, T.A., 2012. Neuroimaging of pediatric posterior fossa tumors including review of the literature. J. Magn. Reson. Imaging 35 (1), 32–47.
Provenzale, J.M., Mukundan, S., Barboriak, D.P., 2006. Diffusion-weighted and perfusion MR imaging for brain tumor characterization and assessment of treatment response. Radiology 239 (3), 632–649.
Rowley, H.A., Grant, P.E., Roberts, T.P., 1999. Diffusion MR imaging. Theory and applications. Neuroimaging Clin. N. Am. 9 (1052–5149), 343–361.
Schaefer, P.W., Grant, P.E., Gonzalez, R.G., 2000. Diffusion-weighted MR imaging of the brain. Radiology 217 (2), 331–345.
Stadnik, T.W., Chaskis, C., Michotte, A., Shabana, W.M., Van Rompaey, K., Luypaert, R., et al., 2001. Diffusion-weighted MR imaging of intracerebral masses: comparison with conventional MR imaging and histologic findings. Am. J. Neuroradiol. 22, 969–976.
Sui, Y., He, W., Damen, F.W., Wanamaker, C., Li, Y., Zhou, X.J., 2015. Differentiation of low- and high- grade pediatric brain tumors with high b-value diffusion weighted MR imaging and a fractional order calculus model. Radiology 277 (2), 489–496.
Sui, Y., Xiong, Y., Xie, K.L., Karaman, M.M., Zhu, W., Zhou, X.J., 2016. Differentiation of low- and high-grade gliomas using high b-value diffusion imaging with a non-Gaussian diffusion model. Am J Neuroradiol [Internet] (Available from: 10.3174/ajnr.A4836).
Szymanski, J., Weiss, M., 2009. Elucidating the origin of anomalous diffusion in crowded fluids. Phys. Rev. Lett. 103 (3), 1–4.
Tien, R.D., Felsberg, G.J., Friedman, H., Brown, M., MacFall, J., 1994. MR imaging of high-grade cerebral gliomas: value of diffusion-weighted echoplanar pulse sequences. Am. J. Roentgenol. 162 (3), 671–677.
Ward, E., DeSantis, C., Robbins, A., Kohler, B., Jemal, A., 2014. Childhood and adolescent cancer statistics, 2014. CA Cancer J. Clin. 64 (2), 83–103.
Weiss, M., 2013. Single-particle tracking data reveal anticorrelated fractional Brownian motion in crowded fluids. Phys. Rev. E Stat. Nonlinear Soft Matter Phys. 88 (1), 1–4.
Winfeld, M., Jensen, J.H., Adisetiyo, V., Fieremans, E., Helpern, J.A., Karajannis, M., et al., 2013. Differentiating high and low grade pediatric brain tumors using diffusional kurtosis imaging. J. Pediatr. Neuroradiol. 2 (4), 301–305.
Yablonskiy, D.A., Bretthorst, G.L., Ackerman, J.J.H., 2003. Statistical model for diffusion attenuated MR signal. Magn. Reson. Med. 50, 664–669.
Yamasaki, F., Kurisu, K., Satoh, K., Arita, K., Sugiyama, K., Ohtaki, M., et al., 2005. Apparent diffusion coefficient of human brain tumors at MR imaging. Radiology 235, 985–991.
Zhang, H., Schneider, T., Wheeler-Kingshott, C.A., Alexander, D.C., 2012. NODDI: practical in vivo neurite orientation dispersion and density imaging of the human brain. NeuroImage 61 (4), 1000–1016.
Zhou, X.J., Gao, Q., Abdullah, O., Magin, R.L., 2010. Studies of anomalous diffusion in the human brain using fractional order calculus. Magn. Reson. Med. 63, 562–569.